POLITECNICO DI TORINO
Repository ISTITUZIONALE

A Periodic Transmission Line Model for Body Channel Communication

(Article begins on next page)

17 October 2022

A Periodic Transmission Line Model for Body Channel Communication

MATTEO BRUNO LODI[ID]**¹, (Graduate Student Member, IEEE), NICOLA CURRELI²,
ALESSANDRO FANTI**[ID]**¹, (Member, IEEE), CLAUDIA CUCCU³,
DANILO PANI¹, (Senior Member, IEEE), ALESSANDRO SANGINARIO**[ID]**³, (Member, IEEE),
ANDREA SPANU¹, (Member, IEEE), PAOLO MOTTO ROS**[ID]**⁴, (Member, IEEE),
MARCO CREPALDI**[ID]**⁴, (Member, IEEE), DANILO DEMARCHI**[ID]**³, (Senior Member, IEEE),
AND GIUSEPPE MAZZARELLA**[ID]**¹, (Senior Member, IEEE)**

¹Department of Electrical and Electronic Engineering, University of Cagliari, 09123 Cagliari, Italy
²Graphene Labs, Istituto Italiano di Tecnologia, 16163 Genova, Italy
³Department of Electronics and Telecommunications, Politecnico di Torino, 10129 Torino, Italy
⁴Electronic Design Laboratory, Istituto Italiano di Tecnologia, 16152 Genova, Italy

Corresponding author: Alessandro Fanti (alessandro.fanti@unica.it)

ABSTRACT Body channel communication (BCC) is a technique for data transmission exploiting the human body as communication channel. Even though it was pioneered about 25 years ago, the identification of a good electrical model behind its functioning is still an open research question. The proposed distributed model can then serve as a supporting tool for the design, allowing to enhance the performances of any BCC system. A novel finite periodic transmission line model was developed to describe the human body as transmission medium. According to this model, for the first time, the parasitic capacitance between the transmitter and the receiver is assumed to depend on their distance. The parameters related to the body and electrodes are acquired experimentally by fitting the bio-impedentiometric measurements, in the range of frequencies from 1 kHz to 1 MHz, obtaining a mean absolute error lower than 4° and 30 Ω for the phase angle and impedance modulus, respectively. The proposed mathematical framework has been successfully validated by describing a ground-referred and low-complexity system called *Live Wire*, suitable as supporting tool for visually impaired people, and finding good agreement between the measured and the calculated data, marking a ±3% error for communication distances ranging from 20 to 150 cm. In this work we introduced a new circuital approach, for capacitive-coupling systems, based on finite periodic transmission line, capable to describe and model BCC systems allowing to optimize the performances of similar systems.

INDEX TERMS Body area network, body channel communication, intra-body communication, propagation model, periodic transmission line.

I. INTRODUCTION

The expressions intra-body communication, human body communication and Body channel communication (BCC) all refer to a short-range communication method that exploits the human body as a transmission medium for electrical signals [1], [2]. The pioneering work of Zimmerman on BCC was motivated by the dream and the imagination of a digital

The associate editor coordinating the review of this manuscript and approving it for publication was Noor Zaman[ID].

interconnected world where the center of communication is the human being [1], [2]. Driven by this idea, BCC can be established relying on two main coupling mechanisms [3]. The signal can be coupled in the body by direct current injection (galvanic coupling - GC) from a transmitter (TX) electrode to a receiver (RX). Alternatively, the near-field coupling of a quasi-electrostatic field between TX and RX electrodes can be used for (capacitive coupling - CC) [3]–[9]. However, the possibility of conveying information in the sub-cutaneous fat at frequencies around 2.45 GHz is currently
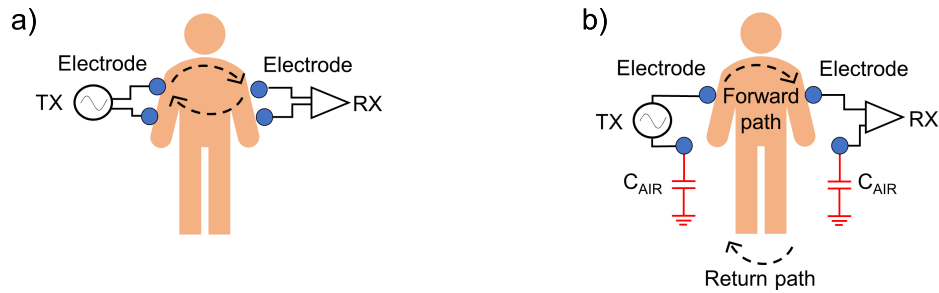
FIGURE 1. a) Galvanic coupling (GC): an electric current is applied between two differential TX electrodes and flows across the tissues to the RX. This determines a primary flow of current through the TX electrode and a secondary path along the inner tissues. b) Capacitive coupling (CC): an electric field is produced by the electrode of the TX. The propagation occurs in the body, through near-field and surface wave mechanism, and onto the air channel, through the return path due to parasitic capacitances.

under investigation [10]–[12]. Therefore, from the comparison of the two mechanisms presented in Fig. 1, despite a higher sensitivity to the external environment [13], the CC stands out thanks to a higher bandwidth and data rate (1-100 Mb/s for CC vs. 1 Mb/s for GC), while ensuring lower path losses and a longer communication distance of maximum 150 cm [3].

BCC enables to interconnect devices located on the body surface and/or implanted, thus representing an appealing technology for the development of Wireless Body Area Network (WBAN). In fact, a BCC system aims to satisfy the requirements of a low energy, small-sized, and light-weight device [14]. In the IEEE 802.15.6 standard, BCC was included as third physical layer, being an effective and energy-efficient candidate [3]–[6], [15], compared to ZigBee and Bluetooth technology. The performance of BCC devices are comparable in terms of data rate while requiring few tenths of nJ/b [3]–[6], [15]. Several examples of BCC applications are related to biomedical applications [4], e.g. systems developed for electrocardiography (ECG) [16], electromyography (EMG) [17], oxymetry [18] but also the communication with implanted devices [3]–[6]. In the biomedical field, the adoption of BCC approaches can disclose novel opportunities by solving well-known issues of clinical biomedical devices [19].

Furthermore, BCC allows the connection of wearable systems with the external objects through simple physical contact [3], [20]. Moreover, the communication may involve even more than one person. In this sense, more people may interact with the same object, or by the contact of more people, for example holding hands, may extend the human channel to allow the interaction with a given target. Therefore, a double communication is established: from the person to the environment, or in the opposite direction, thus creating a digital smart environment [1], [2], [21], [22]. These features make BCC systems similar to passive Radiofrequency Identification (RFID) tags, contactless smart cards, and Near Field Communication (NFC) technologies. However, BCC does not rely on a specific contact point, except the body [21], [22]. This human-centered interactivity

is interesting because the communication is triggered by the person and its willingness to communicate with the external world [2], [3]. The nature of BCC is intrinsically safe, secure and resilient since the data remain confined within the biological medium, making this technology of great interest for applications such as e-payment, work-management, intelligent transportation system, security and entertainment. [23]–[26].

In order to refine and improve the performance of the BCC systems, it is fundamental to have a clear understanding of the fundamentals on-body CC communication. Indeed, despite the knowledge of the features and performances of the available devices, the understanding of the physics and modeling of the signal transmission and propagation in the biologic medium need to be improved. Therefore, this work aim to bridge the gap between the hardware design and the on-body propagation, by developing a model that can deal with the description of the complex mechanism of capacitive coupling, while including the hardware perspective, i.e., the TX and RX components.

In the literature it is possible to find several theoretical models, combined with circuital and/or full-wave (FW) approaches to the human channel modeling [3]–[6], [27]. Some models are capable to seize the essential features of the body channel propagation [28]. An example is the dipole model introduced by Bae *et al.* [8], in which the signal propagation in the CC depends on three distinct mechanism, namely surface wave, reactive radiation, and near-field quasi-static coupling [8], [9]. Regarding the BCC electric circuit model, both lumped and distributed parameter circuits have been investigated [25], [29]–[32]. The lumped parameter model can easily account for the essential electrical properties of different tissues, thus allowing to derive some closed-form expressions for the signal attenuation. However, the flaw of these models is their limited capability to represent realistic and complex cases [3]. Hence distributed models were also introduced. In particular, circuits diagrams were derived by cascading a basic RC cell, in order to analyze the influence of TX-RX distance on signal propagation [25], [33]. Although these simple models allow

deriving simple approximate expressions for the path loss, they are not able to describe the peculiar propagation mechanism of BCC [3]. Therefore, a transmission line model (TLM) using infinite structures was proposed by Callejòn et al. [32] to study the dispersion and attenuation of the body channel considering the electrophysiological properties of the skin as a transverse admittance in the lumped model. However, in this model, the influence of the finite length of the channel on the communication performances is not analyzed in depth. Furthermore, the role and effects of the parasitic capacitance is marginal in the mathematical frameworks, despite its physical relevance [3]. As a result, the state of the art in the field lacks of mathematical models adequate to describe the physics of the on-body propagation using the TLM formalism, while accounting for the influence of the extrinsic parasitic return path on the communication.

Our work aims to bridge the gap for the case of CC mechanism. Indeed, the strategy of developing distributed circuital models is preferable to the extensive, time-consuming and computational-demanding FW approach since the numerical simulations demonstrated that the electric field is almost entirely confined within the skin layer [8], [9], [34], and that the extrapolation of the parasitic capacitance is a non-trivial task [31].

In particular, in this work we developed a mathematical model capable of describing the body-channel propagation using CC devices. The proposed mathematical framework takes into account the strong influence of the environment, typical of capacitive devices, by taking into consideration the relevance of parasitic capacitances in the communication. The proposed distributed model can then serve as a supporting tool for the design, allowing to enhance the performances of any BCC system, especially in terms of working frequency choice, electrode sizing and signal strength.

In this work, the novel TLM model was experimentally validated on the signal propagation with *Live Wire*, a prototype of system which is currently used as indoor navigation aid for blind subjects [35].

The paper is organized as follows. The proposed body-propagation model based on finite periodic transmission line is explained in detail in Sect. II. The circuital representation of CC system is presented in Sect. III. The use-case for the assessment of the model is introduced in Sect. III-A. The model parameters were retrieved from bio-impedentiometric measurements on a set of subjects. The experimental setup is presented in Sect. IV-A, along with the methodological information regarding the numerical fitting performed to derive the model parameters. The explanation of the transmission experiments and the channel characterization tests are reported in Sect. IV-B. The results of the impedance measurements, the fitting and the model validation are given in Sect. V-A. The findings related to the signal transmission using *Live Wire* in several configurations are provided in Sect. V-B. Finally, conclusions are drawn and presented in Sect. VI.
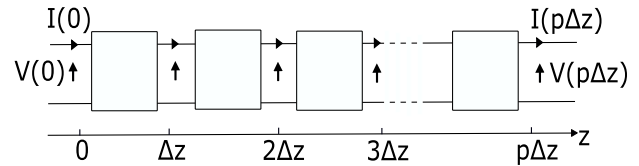

FIGURE 2. Finite periodic transmission line model of an identical repeating p-times two-port network of length Δz.

II. PROPAGATION MODEL

In order to describe, and analyze the propagation of the CC signal, it is possible to connect the physical properties of the on-body propagation channel to its electrical response. Assuming that the skin structure does not vary significantly along a body segment or region, the in- and on-body propagation can be described considering the propagation in a homogeneous structure along the direction of propagation [36], [37]. Since it is possible to derive lumped models for small skin parts, a TLM propagation model can be developed by considering the repetition of a sequence of identical cells. Therefore, the transmission line, having characteristic impedance Z_0, is assumed to be a periodic repetition of a lossy and dispersive RLC cell [37]. Therefore, the connection between the BCC physical mechanism and its electrical response can be done by modeling the channel as a finite periodic sequence of equal two-port networks, each one describing a sufficiently short section of the channel, as in Fig. 2. The complete circuit can be described using voltages (V) and currents (I) at the interfaces. Setting

$$\underline{W}(q\Delta z) = \begin{bmatrix} V(q\Delta z) \\ I(q\Delta z) \end{bmatrix} \tag{1}$$

where Δz is the length of the section and $q = 1, 2, \ldots p$, being p the total number of repeating unit. By using the transmission matrix of the unit cell $\underline{\underline{T}}$

$$\underline{\underline{T}} = \begin{bmatrix} A & B \\ C & D \end{bmatrix} \tag{2}$$

we can write[1]

$$\underline{W}(p\Delta z) = \underline{\underline{T}}^p \cdot \underline{W}(0) \tag{3}$$

Eq. (3) can be given a closed-form expression using the eigenvalue decomposition of $\underline{\underline{T}}$, i.e., the eigenvalues λ and the eigenvectors $\underline{h}$, solutions of

$$\underline{\underline{T}}\,\underline{h} = \lambda \underline{h} \tag{4}$$

The eigenvalues equation is

$$\lambda^2 - (A+D)\lambda + 1 = 0 \tag{5}$$

and therefore the product of the eigenvalues (λ) is equal to two. We can therefore let $\lambda_1 = e^{-jk\Delta z}$, $\lambda_2 = e^{jk\Delta z}$, where k is a complex number, and obtain

$$\lambda_1 + \lambda_2 = e^{-jk\Delta z} + e^{jk\Delta z} = 2\cos k\Delta z = A + D \tag{6}$$

[1]For $q < 0$, we let, in Eq. (3), $\underline{\underline{T}}^q = \underline{\underline{T}}^{-|q|} = (\underline{\underline{T}}^{-1})^q$. Note that $\underline{\underline{T}}$ is always nonsingular since $det(\underline{\underline{T}}) = \overline{1}$.

The eigenvectors can be normalized and therefore expressed as $\underline{h} = \begin{bmatrix} 1 \\ y_i \end{bmatrix}$, where

$$y_1 = \frac{e^{-jk\Delta z} - A}{B}$$

$$y_2 = \frac{e^{jk\Delta z} - A}{B} \qquad (7)$$

Using the eigenvectors we can represent $\underline{\underline{T}}$ as

$$\underline{\underline{T}} = \underline{\underline{H}} \cdot \begin{bmatrix} e^{-jk\Delta z} & 0 \\ 0 & e^{jk\Delta z} \end{bmatrix} \underline{\underline{H}}^{-1} \qquad (8)$$

where $\underline{\underline{H}} = \begin{bmatrix} 1 & 1 \\ y_1 & y_2 \end{bmatrix}$ and $\underline{\underline{H}}^{-1} = \frac{1}{y_2 - y_1} \begin{bmatrix} y_2 & -1 \\ -y_1 & 1 \end{bmatrix}$, obtaining

$$\underline{\underline{T}}^q = \underline{\underline{H}} \cdot \begin{bmatrix} e^{-jkq\Delta z} & 0 \\ 0 & e^{jkq\Delta z} \end{bmatrix} \underline{\underline{H}}^{-1} \qquad (9)$$

From (9) it is possible to derive the voltages and the currents on the channel.

Since the unit cell is specular, i.e., symmetrical [38], $A = D = \cos(k\Delta z)$ [see (6)], so that

$$y_1 = -\frac{j \sin(k\Delta z)}{B}$$

$$y_2 = \frac{j \sin(k\Delta z)}{B} = -y_1 \qquad (10)$$

and obtaining

$$\underline{\underline{H}}^{-1}\underline{W}(0) = -\frac{1}{2y_1} \begin{bmatrix} -y_1 & -1 \\ -y_1 & 1 \end{bmatrix} \begin{bmatrix} V(0)| \\ I(0) \end{bmatrix}$$

$$= \frac{1}{2} \begin{bmatrix} 1 & 1/y_1 \\ 1 & -1/y_1 \end{bmatrix}$$

$$= \frac{1}{2} \begin{bmatrix} V(0) + \dfrac{1}{y_1}I(0) \\ V(0) - \dfrac{1}{y_1}I(0) \end{bmatrix} = \begin{bmatrix} V^+ \\ V^- \end{bmatrix} \qquad (11)$$

where V^+ and V^- are the propagating and reflected voltage waves, respectively. It follows that

$$\underline{W}(z) = \underline{\underline{H}} \cdot \begin{bmatrix} V^+ e^{-jkq\Delta z} \\ V^- e^{jkq\Delta z} \end{bmatrix} \qquad (12)$$

i.e.,

$$V(q\Delta z) = V^+ e^{-jkq\Delta z} + V^- e^{jkq\Delta z}$$

$$I(q\Delta z) = y_1 \left[V^+ e^{-jkq\Delta z} - V^- e^{jkq\Delta z} \right] \qquad (13)$$

which is clearly analogous to the propagation along a transmission line.

A. CHANNEL ANALYSIS

The electrical response of the on-body channel depends on the parameters k and y_1 [see Eq. (11)], based on the physical behavior of the unit cell. The equivalent circuit representing the body channel is shown in Fig. 3.
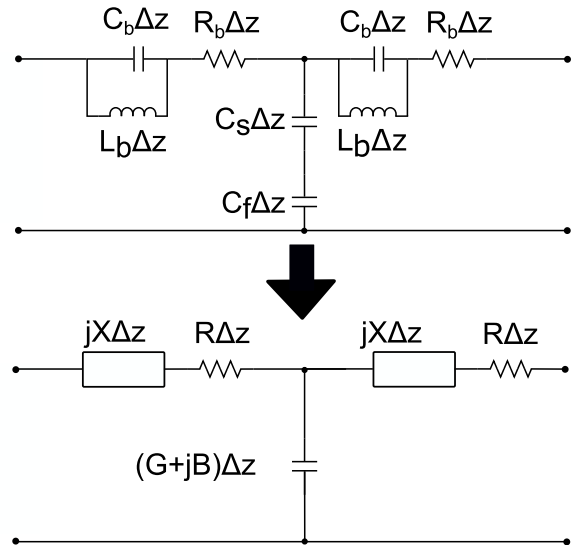

FIGURE 3. Circuital representation of the unit cell for the periodic transmission line model of a body segment involved in capacitive coupling, assuming the field propagation is confined within the skin and air. In this work $\Delta z = 2$ cm.

Given the capacitive coupling mechanism and the low working frequency of BCC devices, the body propagation is assumed to be confined in the superficial skin layers (i.e., epidermis, dermis and subcutaneous layers) [3], [34]. On the skin, longitudinal and transverse paths can be recognized as relevant to the signal propagation, as underlined in [25], [32]. The propagation of the CC signal in the body channel is described by assuming the skin to be homogeneous along the propagation direction and, hence, the periodic transmission line formalism can be applied [36], [38]. The single cell considered in this study is shown in Fig. 3. The inductance L_b accounts for the radio-frequency currents induced in the body along the direction of propagation, whilst C_b accounts for the inter-electrode coupling and the parasitic effects of the environment, and R_b is the resistance of the body segment. The signal in the transverse section is supposed to flow as an electric current through the subject skin, via the skin capacitance C_s, and then to the ground by a parasitic capacitance C_f between the skin and the external ground. The skin layer is modeled as a lossy capacitor with capacitance per unit length C_s, in Fm^{-1} [25], [32], [39]–[41]

$$C_s(\omega) = \epsilon_\infty + \sum_{i=1}^{4} \frac{\Delta \epsilon_i}{1 + \left(j\omega\tau_i\right)^{(1-\alpha_i)}} + \frac{\sigma}{j\omega\epsilon_0}$$

$$= \epsilon_0(\epsilon_s' - j\epsilon_s'') \qquad (14)$$

where ϵ_∞ is the dielectric permittivity at optical frequencies, $\Delta\epsilon$ is defined as the difference between the static and the optical permittivities (i.e., $\Delta\epsilon = \epsilon_s - \epsilon_\infty$), τ is the relaxation time in s, as found in [39]–[41] for the wet skin. The terms ϵ_0 is the vacuum dielectric permittivity in Fm^{-1} and $\omega = 2\pi f$ is the angular frequency.

The transmission matrix of the circuit of Fig. 3 is [42]:

$$\underline{T} = \begin{bmatrix} 1+(R+jX)(G+jB)\Delta z^2 & 2(R+jX)\Delta z+(R+jX)^2(G+jB)\Delta z^3 \\ (G+jB)\Delta z & 1+(R+jX)(G+jB)\Delta z^2 \end{bmatrix} \quad (15)$$

Therefore, (6) becomes

$$\cos(k\Delta z) = A = 1 + (R+jX)(G+jB)\Delta z^2 \quad (16)$$

and, for negligible Δz, a Taylor expansion of the right hand side gives the equation

$$-\frac{1}{2}k^2 = (RG - XB) + j(RB + GX) \quad (17)$$

If the network was lossless, the equation for k would be $k^2 = 2XB$, so that we have actual propagation for $XB > 0$. Since $B > 0$, we have propagation as long as the series LC in Fig. 3 has an inductive nature, i.e., $X > 0$. This is true in the frequency range of interest. However, as the frequency increases, the propagation would be cut-off and the signal strength would be attenuated when the capacitive susceptance becomes larger than the inductive one (see Fig. S2 of the Supp. Material). In the real lossy case, we have small losses ($R \ll |X|$, $G \ll |B|$) so that (17) can be written as

$$k^2 = 2XB - 2j(RB + GX) \quad (18)$$

and its right hand side is just below the real axis. Therefore, we have a (lossy) propagation for $XB > 0$, i.e., in the frequency range of interest (and also above it, up to a frequency of several tens of MHz, where X becomes negative).

For $\Delta z \to 0$, Eq. (13) becomes the standard solution of telegrapher equations [42], with the propagation constant given by (18) and characteristic impedance equal to

$$Z_0 = \frac{1}{y_1} \simeq \frac{B}{-jk\Delta z} \simeq \frac{2R+jX}{-jk}$$
$$\simeq -\frac{2X}{k} + 2j\frac{R}{k} \quad (19)$$

which could be approximated as $-\frac{2X}{k}$, since its small imaginary part has no physical effects [43].

III. PROPAGATION BEHAVIOR IN CC SYSTEMS

The analytical description of the body channel as a transmission line provides the knowledge of its propagative behavior and characteristic impedances. It is worth noting that this model can describe the propagation of the signal in a given body segment, providing a quantitative basis for the improvement of any BCC device.

A. LIVE WIRE DEVICE

As a use-case for the assessment of our BCC model, we chose to consider the *Live Wire* [35], [44]. *Live Wire* has been implemented by using discrete components, a choice shared with similar BCC devices [2], [45], [46], rather than developing a custom complementary metal oxide semiconductor (CMOS) integrated circuit [33], [47]–[50]. The *Live Wire* system is shown in the block diagram of Fig. 4.
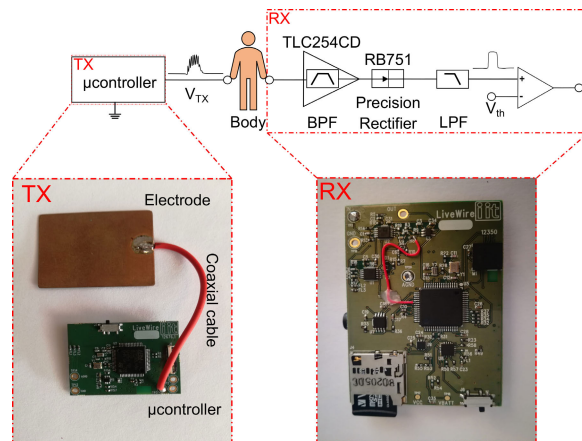

FIGURE 4. Block diagram of the device *Live Wire*. TX: Transmitter, RX: Receiver.
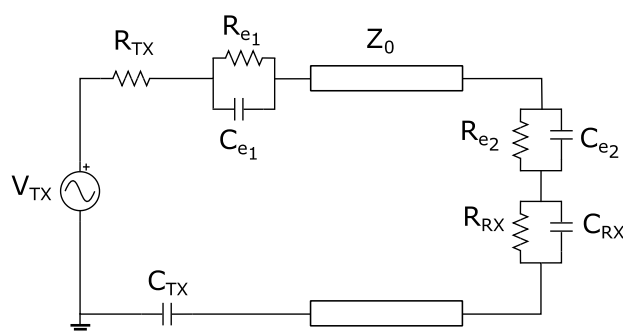

FIGURE 5. Equivalent circuital representation of the BCC transmission channel. The transmission line is obtained from the network of Fig. 2 assuming the unit cell of Fig. 3.

The details about the design and functioning about the *Live Wire* device can be found in [35], [44]. In the following we report the essential information required to understand the validation of the circuital representation in Fig. 5 and the experimental communication tests.

The TX is a battery powered module, featuring the STM32L486 microcontroller (ST Microelectronics, Geneve, CH). The TX electrode is connected to a low-impedance (50 Ω) general purpose input/output (GPIO) pin of the microcontroller. The *Live Wire* system adopts a self Synchronized-On-Off-Keying (S-OOK) strategy because of its low average power consumption of by the TX (100 mW on average) [3]–[6], [35], [44], [51]. The TX signal, V_{TX}, is a 670 kHz square wave, scaled by non coherent impulses [44]. The carrier frequency was selected considering the trade-off between the possibility to adopt the system as an aid for blind subjects, while respecting safety regulations and preventing, as much as possible for a CC device, the environmental interferences (e.g., to other electronic devices) [3]. The signal is coupled to the human body by means of a 5.5 cm × 3.6 cm copper plate acting as a TX electrode (Fig. 4). Even though the electrode area is quite large (about 20 cm^2), compared to the active area of commercial gelled electrodes for biopotentials recordings, dry electrodes (e.g., the textile ones)

present areas up to $24 \, \text{cm}^2$ [52] and more [53]. The size is comparable to the whole-area (including the support) of several commercial electrodes too for recording (e.g., COVIDIEN H49P or FIAB F9079), and smaller than several electrodes for functional stimulation. The TX electrode can be in direct contact with the body or garments, and it is short-circuited to the external ground to ensure both the direct and return paths [35], [44]. Downstream, the signal propagates in the human body to the receiver unit thanks to a pick-up electrode made up of a $2 \, \text{cm} \times 2 \, \text{cm}$ copper plate. The size of the TX and RX electrodes were chosen considering the trade-off between the dimension of the ground electrodes and the signal strength, as underlined in [3] (see Sect. SM3 of the Supp. Material). The demodulation and synchronization are performed through a software routine running on the microcontroller, which verifies the I/O V_{RX} status, thus reducing the overall hardware complexity. The *Live Wire* system requires one 150 mAh Li-Po battery (nominally 3.6 V) and two ADP1712 (Analog Devices, Norwood, MA, USA) linear voltage regulators for the power supply module.

B. CIRCUITAL REPRESENTATION

The application of the model to the *Live Wire* device is shown in Fig. 5, where the transmitter voltage (V_{TX}), the receiver impedance (Z_{RX}), composed of a capacitance (C_{RX}) with a resistance (R_{RX}) in parallel and the contact impedances between the electrode and the skin in TX and RX (Z_{e_1} and Z_{e_2} respectively) are shown.

The model has then been used to calculate the RX voltage V_{RX}, which is the actual output of the communication using the human body as transmission medium. The voltage at the RX can be derived moving from the calculation of the series impedance between the RX electrode and the receiver impedance Z_{RX}, i.e.,

$$Z_H = Z_{e_2} + Z_{RX} \tag{20}$$

where the impedance of the receiver, shown in Fig. 4, is the parallel between a resistance R_{RX} of 1 MΩ and a capacitance C_{RX}, due to a plastic case which separates the metal electrode and the printed circuit board (PCB). In mathematical terms C_{RX} can be estimated as

$$C_{RX} = \frac{\epsilon_0 \epsilon_r A}{t} \tag{21}$$

where the dielectric permittivity of the plastic material is $\epsilon_r = 2$, A is the plates area (m^2) and t, in m, is the distance between the electrode and the PCB. For our case, the electrode size is $5.5 \, \text{cm} \times 3.6 \, \text{cm}$ and the plates are 2 mm distant, hence, the capacitance is about 17.5 pF.

Knowing the body impedance Z_0 and the propagation constant k derived from the periodic TML model, by using (19) and (18), with $\Delta z = 2$ cm, respectively, the impedance seen from the line, Z_{IN} can be evaluated as

$$Z_{IN} = Z_0 \frac{Z_H \cos(kd) + j Z_0 \sin(kd)}{Z_0 \cos(kd) + j Z_H \sin(kd)} \tag{22}$$

where d is the distance between electrodes. Then, the current flowing in the Thevenin equivalent is derived as follows

$$I_0 = \frac{V_G}{Z_{TX} + Z_{e_1} + Z_{IN}} \tag{23}$$

where Z_{TX} is the transmitter impedance, defined as

$$Z_{TX} = R_{TX} + \frac{1}{j \omega C_{TX}} \tag{24}$$

The term R_{TX} is equal to 50 Ω, as experimentally verified, and the radiation losses of the electrode are negligible at the working frequency of 670 kHz. This contribution should be considered due to the ambiguous electrode-antenna behavior observed elsewhere in the literature [3].

The value of the parasitic impedance for the extrinsic return path, C_{TX}, in pF, is a largely variable quantity (from tenths pF to tens of pF), according to the literature, and, furthermore, it has been often considered as a function of the working frequency and of the size of the TX or RX electrodes [20], [31]. However, its explicit dependence from the environment and the working configurations is still an open issue. Provided that, for CC systems, the environments has a considerable influence on the secondary path, it is reasonable to assume that the parasitic capacitance depends on the TX-RX distance d, in m, employing the following second-order polynomial function

$$C_{TX}(d) = c_0 + c_1 d + c_2 d^2 \tag{25}$$

where c_2 is equal to $4 \, \text{pFm}^{-3}$, c_1 is $3 \, \text{pFm}^{-2}$ and, finally, $c_0 = 1 \, \text{pFm}^{-1}$. The assumption of $C_{TX} = C_{TX}(d)$ should be interpreted considering that as TX-RX distance increases, the effective area available for the capacitive return path increases too [3]. Different models were tested, namely a constant capacitance value, a first, second and third order polynomial function. However, among the tested functions, the rate of variation of $C_{TX}(d)$ which allows to best fit the experimental data was Eq. (25).

Then, the voltage in the equivalent circuit is derived as

$$V_0 = Z_{IN} I_0 \tag{26}$$

Hence, the voltage at the end of the body segment can be evaluated with the following transport equation

$$V(d) = V_0 \cos(kd) - j Z_0 I_0 \sin(kd) \tag{27}$$

The current flowing from the transmission line is

$$I(d) = I_0 \cos(kd) - j \frac{1}{Z_0} V_0 \sin(kd) \tag{28}$$

Finally, the voltage on the receiver unit is

$$V_{RX} = Z_{RX} I(d) \tag{29}$$

The voltage V_{RX} has been derived from the proposed model by calculating it using the circuital representation in Fig. 5 and relying on the periodic TLM representation of the human body. The obtained quantity was compared to the experimental results in order to validate the model. It must be

pointed out that the quantities Z_{TX} and Z_{RX} are known or can be estimated, whilst the value of Z_{e_1} and Z_{e_2} depend on the type of electrodes used and on the subject skin. Furthermore, the value of Z_0 cannot be estimated from the model unless the line parameters, i.e., the single cell RLC components, are known or found from experimental analysis.

IV. EXPERIMENTALS

A. IMPEDANCE MEASUREMENTS

In order to validate the TLM and circuital representation proposed for the signal transmission, the possible role on the propagation of the impedances of both the electrodes and the dielectric properties of the biological medium were investigated.
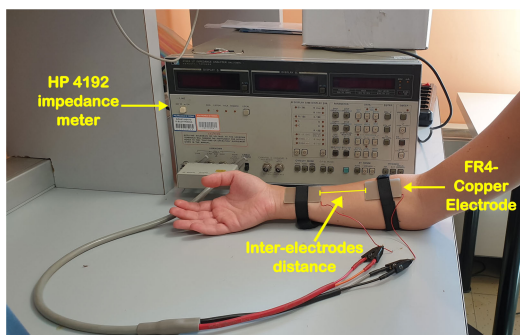

FIGURE 6. Experimental setup for the measurement of the forearm impedance.

To cover the range of working frequencies of BCC, the contact bio-impedance measurements were performed from 50 kHz to 1 MHz, with a 50 kHz span, using a HP 4192A (Keysight Technologies, Santa Rosa, CA, USA) impedance meter, as shown in Fig. 6. The instrument was calibrated at the upper frequency value of 1 MHz. Two FR4-copper electrodes were placed on the anterior forearm, with the metal faces in contact with the skin. The TX and RX are not present in this configuration, thus implying that the measured impedance is the effective impedance without considering V_G (voltage generator), Z_{e_1}, Z_{e_2} in Fig. 5. In particular, one electrode is placed near the wrist and the other one near the elbow, as shown in Fig. 6. On ten voluntary subjects, the impedance was computed as the mean over three consecutive measurements, to smooth over noise and measurement errors. The anthropometric characteristics of the subjects are reported in Tab. 1. The study was performed following the principles outlined in the Helsinki Declaration of 1975, as revised in 2000. Subjects were informed about the aim of the study, and they provided their informed consents. For all the subjects the inter-electrode distance was set to 2 cm, 5 cm and 10 cm.

To evaluate the unknown parameters of the body path, i.e., L_b, C_b, R_b, C_f, and of the contact impedance, i.e., R_{e1}, C_{e1}, R_{e2}, C_{e2}, a Matlab routine (The MathWorks Inc., Natick MA, USA) was implemented to fit the model with the experimental data of the contact impedance measurements. Among

TABLE 1. Biometric data of the subjects tested in bio-impedentiometric measurements.

Sub. ID	Gender	Age (y)	Height (cm)	Weight (kg)
S1	M	25	187	82
S2	F	24	165	60
S3	M	25	183	65
S4	F	18	162	57
S5	F	25	160	60
S6	F	24	162	58
S7	M	24	175	68
S8	F	24	160	62
S9	M	25	180	70
S10	M	25	170	71

the available fitting strategies, the fitting was performed by using an in-house Genetic Algorithm (GA) to minimize the difference between the square of the experimental impedance and the analytical impedance values, i.e.,

$$F = \sum_{i=1}^{M} \left| Z_{exp}(f)^2 - Z_{model}(f)^2 \right| \tag{30}$$

where M is the number of frequency points f from 1 kHz to 1 MHz, Z_{exp} is the measured impedance and Z_{model} is the impedance calculated by using the proposed model. The initial population was set to 10^5 individuals, the maximum number of iteration was fixed to 250, whilst the crossover and mutation probabilities were set to 0.5.

B. CHANNEL CHARACTERIZATION AND TRANSMISSION MEASUREMENTS

The BCC is assessed by measuring the Signal-to-Noise Ratio (SNR) and the communication performances in several cases, as shown in Fig. 7 [54]. The model is used to understand and interpret these experimental situations. The *Live Wire* device is used in the experiments [35], [44].

This measurement requires to know the voltage at the receiver and the noise voltages. To make these data available to the user, RX sends these informations via Bluetooth to the PC. The receiver output is a voltage encoded in 12 bits (V_{12bit}), so it is converted in volt (V_{Volt}) in post-processing as follows:

$$V_{Volt} = \frac{V_{12bit} V_{REF}}{(2^{nbit} - 1)A} \tag{31}$$

where V_{REF} is voltage reference of the ADC (2.83 V) and the signal amplification is $A = 22$.

SNR in dB is then measured as:

$$\text{SNR} = 10 \log \left(\frac{P_s - P_n}{P_n} \right)$$
$$= 10 \log \left(\frac{\frac{(V_s - V_o)^2}{R_{RX}} - \frac{(V_n - V_o)^2}{R_{RX}}}{\frac{(V_n - V_o)^2}{R_{RX}}} \right) \tag{32}$$

where P_s and P_n are signal and noise power respectively, whilst V_s and V_n are signal and noise voltage respectively,
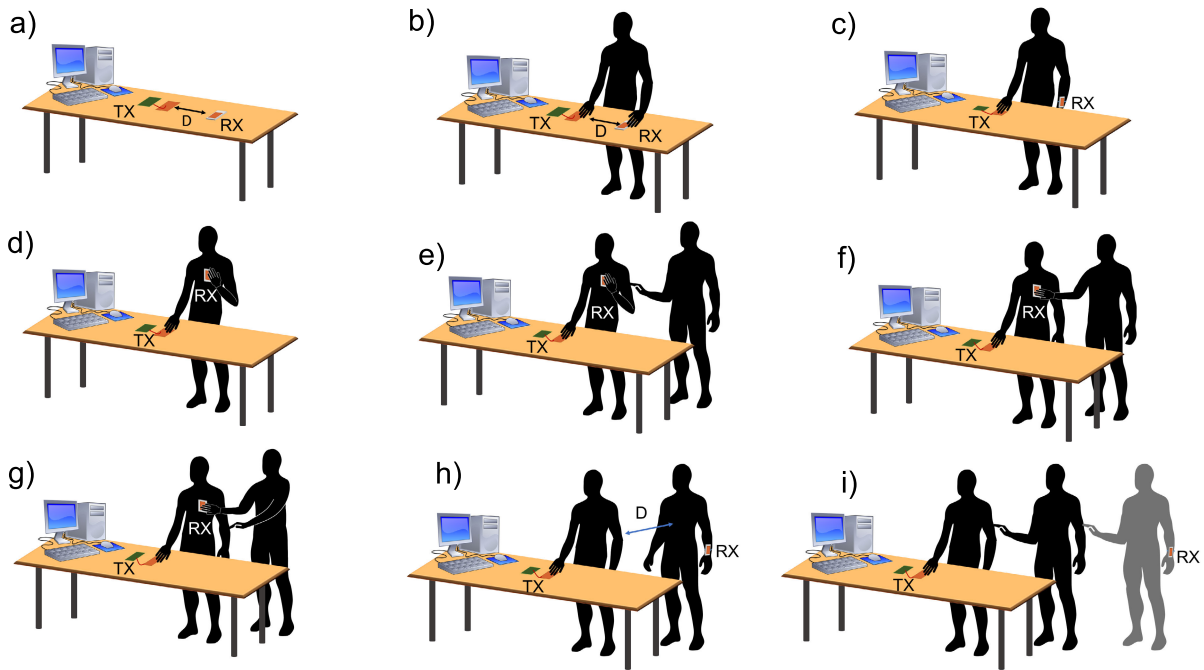
FIGURE 7. a) The signal propagates in air at different distances D between TX and RX. b) The signal propagates via BCC at different distances D between TX and RX. c) Single person measurement: the subject wears RX (in this case on the left wrist) and touches TX with the hand. d) Body shielding test, configuration 1: the person wearing RX touches with one hand TX and the other is put on the receiver. e) Body shielding test, configuration 2: the person wearing RX touches with onehand TX and the other is put on the receiver. The person is in physical contactwith another subject. f) Body shielding test, configuration 3: The person wearing RX touches with one hand TX. A second subject puts the hand on RX. g) Body shielding test, configuration 4: the person wearing RX touches with one hand TX. A second subject puts the hand on RX. The subjects are in physical contact. h) The signal propagates via BCC at different distances D between the two subject which are not in physical contact. i) People chain test: The two subjects are in physical contact. The person touching TX does not wear RX, which is placed on the body of another subject. Signal propagates through the bodies of the subjects. The first person of the chain touches TX whereas the last wears RX. The chain starts from one person and then one person per time is added up to a total of six. Here three people chain example is shown.

V_o is voltage offset of the RX ADC and R_{RX} is the input resistance of the receiver, equal to 1 MΩ.

The SNR is a simple method to measure the signal level and it allows to derive information about path gain, however it is not strictly representative of the actual communication performances of the devices, the packet error rate (PER) and total error rate (TER) were analyzed as figure of merits for the actual communication between TX and RX. In the specific four different scenarios may occur, i.e. the packet CRC is correct (packet correctly received), incorrect CRC but correct packet length (packet error), only the first or central part of the packet is received (synchronization error), or the packet is not received. In order to assess TER and PER the following relations have been used:

$$PER = \frac{\# \text{ Uncorrect Packets}}{\# \text{ Correct Packets}} \qquad (33)$$

$$TER = 1 - \frac{\# \text{ Correct Packets}}{\# \text{ Total packets sent}} \qquad (34)$$

For PER calculation only packets with incorrect CRC and correct length are considered. Moreover, in these tests the total packets sent were 500.

The following scenarios have been evaluated for the SNR, TER and PER, namely:

- The near field coupling in air was tested by placing the TX and RX on a table at a variable distance $d5$, as shown in Fig. 7(a);
- The difference between air communication and the case where the subject's body acts as transmission medium was investigated for the same distance, as depicted in Fig. 7(b);
- The on-body propagation was studied when the RX was worn on the subject's arm, by varying the distances between TX and RX, as presented in Fig. 7(c);
- The SNR levels and the transmission were assessed when the signal can be shielded or shunted [44]. Four distinct case were considered. At first, it was tested the case when the subjects wear the RX on their chests and touch themselves with their own hand while contacting the TX, as shown in Fig. 7(d) (Self Hand, No Touch). The effects of the body shielding were studied when another subject touches the subject equipped with the RX, as shown in Fig. 7(e) (Self Hand, Touch). Then, it was investigated the configuration in which this second subject covers the RX with his hand, as shown in Fig. 7(f) (No Self Hand, No Touch). Finally, it was assessed the case when the second subject covers the RX with the hand while touching the subject in
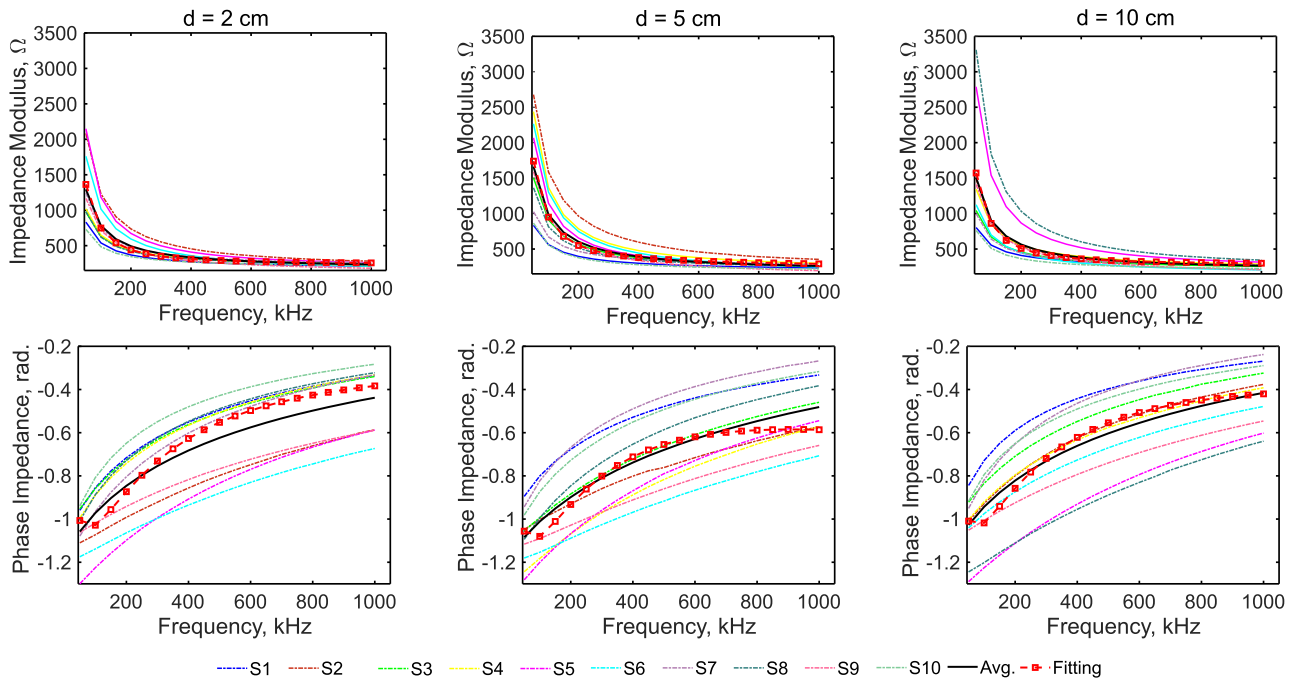
FIGURE 8. Modulus and phase of the impedance between the TX and RX electrodes placed on the anterior forearm at a distance of 2 cm, 5 cm and 10 cm.

contact with TX, as shown in Fig. 7(g) (No Self Hand, Touch). The distance between the RX and the hand was varied up to 15 cm in a direction normal to the metal surface of the RX;

- In Fig. 7(h), it is represented the case of No Touch Propagation, i.e., the possible transmission of signal when one subject is in contact with the TX, but another person, at a distance D, wears the RX. This very critical but relevant case was studied to assess the influence of the capacitive return path varying the distance between the two subjects;
- The attenuation of a chain of people, from one to six, was investigated by employing the configuration shown in Fig. 7(i).

V. RESULTS

A. IMPEDANCE FITTING AND MODEL VALIDATION

The parameters needed to validate the model were derived from the bio-impedances measured as described in Sect. IV-A. The results of the modulus and phase of the impedance measured on ten different subjects for three different inter-electrode distances are reported in Fig. 8. For all distances between TX and RX, the modulus of the impedance between the two electrodes decreases as frequency increases, being almost constant up above 500 kHz, i.e., for the working frequencies of CC systems, such as the *Live Wire* device. On the other hand, the phase tends to increase monotonically with the frequency. The variability of the complex impedances between subjects is quite noticeable, with a 30% of uncertainty typical of human dielectric properties [34], [55].

TABLE 2. Results from the fitting of the proposed transmission line model to the impedance measurements.

Parameter	$d = 2\,\text{cm}$	$d = 5\,\text{cm}$	$d = 10\,\text{cm}$
R_{e1}, kΩ	3.41	4.65	3.93
C_{e1}, nF	2.37	1.85	0.03
R_{e2}, kΩ	0.32	0.68	4.11
C_{e2}, pF	37.0	68.3	2006
L_b, nH	0.975	0.978	0.539
C_b, nF	2.37	1.85	0.03
R_b, Ω	9880	10	532
C_f, pF	40.8	98.4	38.7

From Fig. 8, the unknown model parameters were derived by numerical fitting using the cost function introduced in Eq. (30). The results for the three inter-electrode distances are reported in Tab. 2. They reveal how the spacing between the resistances R_{e_1}, R_{e_2} and the capacitance C_{e_2} proportionally increases by increasing the electrode distance. On the other hand, the capacitance C_{e_1}, C_b and C_f decreased. Furthermore, the variation of L_b can be explained. Indeed, between the values derived for $d = 2\,\text{cm}$ and $d = 5\,\text{cm}$ there is a 0.3% difference, within the tolerance of the GA. The inductance value derived for $d = 10\,\text{cm}$ is about 0.55 times lower than the one retrieved for a body segment a half and a fifth long, thus implying that the induced currents flowing in the skin decreases as the length of the transmission line increases, which agrees with theoretical and full-wave results of other literature works [3], [8], [9], [34]. As regards the values of R_b, it must be underlined that this quantity accounts for the ideal electrical current path if the signal does
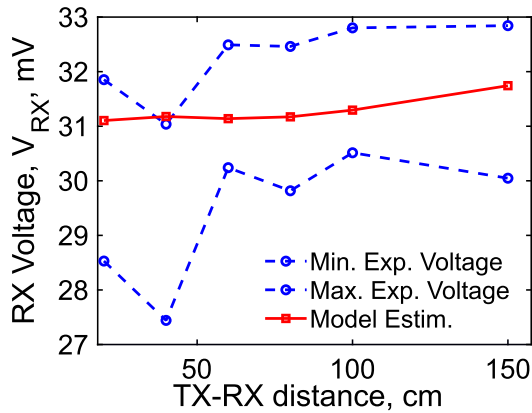
FIGURE 9. Values of maximum and minimum voltage recored at the receiver for different distances between TX and RX. The curves for the min. and max. RX voltages are the average of ten experiments. The distances are considered moving the RX from the arm (minimum of 10 cm) to the chest (maximum 150 cm).

FIGURE 10. The signal propagation in air and through the body analyzed for distances between TX and RX ranging from 0 cm to 50 cm between TX and RX.

not penetrate along the transverse section of the skin [32]. However, even though R_b is supposed to retain this physical meaning, it has been reported that its value is related with the experimental conditions, the type of coupling and the electrodes configuration and hence it has a range of variation of hundreds of ohms [25], [31].

The fitting curves calculated with the results reported in Tab. 2 are shown in Fig. 8. It can be noticed that the average absolute error on the module is 24.38 Ω, 27.75 Ω and 28.74 Ω for 2 cm, 5 cm and 10 cm, respectively. The average absolute error on the phase is 3.29°, 2.13° and 1.88° for 2 cm, 5 cm and 10 cm respectively. Using the dielectric dispersion model of the dry skin lead to more than 60° on the phase impedance and about 100 Ω for the modulus. As previously underlined by [3], [32], the hydration effects of the skin causes the phase constant to increase with frequency, as can be observed from Fig. 8, or derived from Eq. (18), causing the degradation of modulated signals, thus limiting the available bandwidth. This is due to the one order of magnitude difference between the electromagnetic properties of the wet and dry skin across the whole frequency range [39], [56]–[59]. Furthermore, it should be stressed that, using the simple RC model of Wang *et al.* [25], the deviation from the measured V_{RX} is more than 50%, and so, if C_{TX} = const, the calculated receiver voltage would decrease with increasing TX-RX distance. As a result, the proposed periodic transmission line model is capable of describing the behavior of the body impedances with respect to frequency and TX-RX distance.

Given the parameters of Tab. 2 and the estimated values of the RX and TX components, the circuit of Fig. 5 was used to calculate the values of voltage at the receiver in different configurations, taking into account the space dependency of the parasitic capacitance between TX and RX. The results obtained by the study of the complete model are shown in Fig. 9, where the average minimum and maximum experimental voltages measured for the ten subject on bare skin are reported. It can be noticed that the
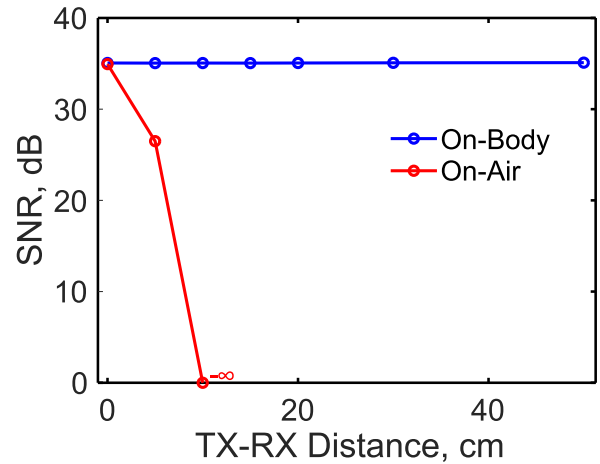
value of voltage at the RX site estimated using the developed TML are able to predict V_{RX} which fells within the ± 5 mV experimental deviations of the measured data. A slight exception is noticed for the case of an inter-electrode distance of d = 40 cm, which exceeds the maximum experimental voltage value of only 0.45%. This error is probably due to the polynomial approximation of the ground return capacitance of the transmitter (see Eq. (25)). It is important to underline that, to the best of the authors' knowledge, the dependence of the return path on the distance has been used for the first time in this work and can successfully explain the lack of a direct dependence between RX voltage and distance. The fitted parameters of TL used in this model are fixed and correspond to a TX-RX distance of 10 cm, i.e., five times the size Δz of the unit cell. For increasing distances, it would be expected that these parameters change, but the model proposed is robust with respect to these variations. Indeed, if the TLM parameters remain in the expected range of values, the voltage output variations are negligible. Therefore the model developed can reliably describe the BCC communication.

B. SNR AND SIGNAL TRANSMISSION

In the first scenario, the BCC propagation was tested with and without the body, as shown in Fig 7.(a) and 7.(b). The goal of this test was to demonstrate the range of distances enabling capacitive transmission without the presence of the human body, i.e., when the signal propagates via the parasitic capacitance C_{TX} between the RX and the TX, and when the body acts as transmission medium. The comparison of the SNR in the case of Fig. 7.(a)-(c) demonstrates that, for small distances below 5 cm, the signal propagates from the TX to the RX regardless the communication channel (whether it is the air or the body). This is coherent with the physical mechanism of the capacitive coupling and the proposed model. As shown in Fig. 10, in the presence of the body
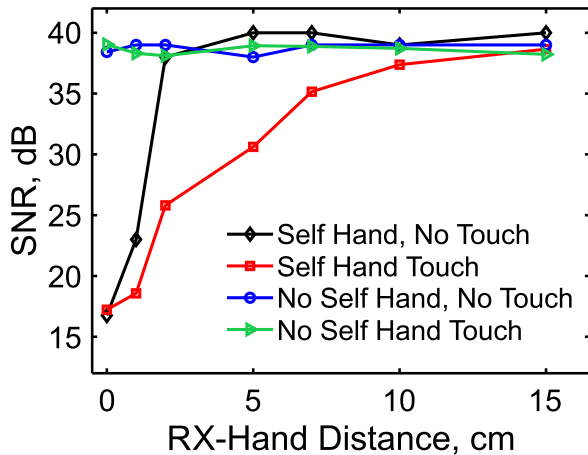
FIGURE 11. SNR over TX-hand distance for four different configurations. a) PER measurements in the case of body shielding evaluation. b) TER measurements in the case of body shielding evaluation. (Self Hand, No Touch - Fig. 7(d); Self Hand, Touch - Fig. 7(e); No Self Hand, No Touch - Fig. 7(f); No Self Hand, Touch - Fig. 7(g))

FIGURE 12. SNR for the No Touch propagation test in four different configuration of the subject. For distances above 100 cm, the SNR was not defined. Hence no communication between the TX and RX unit occurs.

channel between the TX and RX, the electromagnetic signal can propagate with lower attenuation than in the air channel, thus realizing a guided-like propagation. When the distance increases, in the case of on-air propagation, the signal levels quickly decrease to zero. Indeed, the transmission does not occur at all for $d > 5$ cm. On the other hand, the on-body communication retains the signal attenuation around 35 dB for all the distances analyzed in this test. These results can be explained by using the proposed model and the response of the circuit scheme shown in Fig. 5. If the periodic transmission line representing the body is removed from the circuit in Fig. 5, the signal in the air path attenuates as distance increase (5 dB/cm) due to the increasing value of the parasitic capacitance C_{TX}, according to Eq. (25). This results in a drastic reduction of the SNR. The presence of the body establishes an almost constant signal levels at the RX site (about 40 dB $\pm$ 0.12 dB).

Remembering that the BCC device under analysis was developed as a tool for blind subjects [35], it is necessary to investigate the influence of the environment and the possible disturbing effect of body configurations or the interaction with other subjects. Therefore, the effect of body shielding in different configurations was evaluated for the cases presented in Fig. 7(d)-(g). The signal attenuation, in terms of SNR, was assessed in four cases when the same subject or another one place their hand over the RX. The results are shown in Fig. 11. The SNR remains almost constant (in the range between 37-40 dB) in the case the hand touching RX belongs to another person. On the other hand, when the person touching TX lays the own hand over the RX electrode, a shielding effect appears, causing up to 22 dB of reduction in the SNR. When the distance between the RX and the covering hand increases, the SNR levels returns to 40 dB. The SNR increases by 100% in a 10 cm range when the hand of the subject wearing the RX is moved away from the TX. According
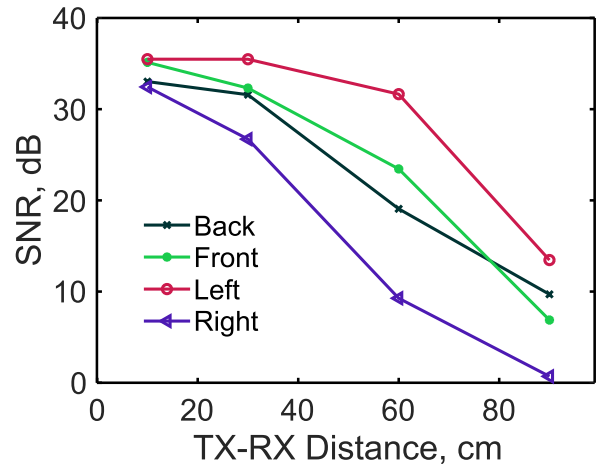
to our transmission line model, the 50% reduction in SNR values observed in the cases of self-touch can be explained considering that the presence of the hand on the RX induces an anti-phase signal whose propagation degrades the voltage wave. The influence of the destructive signal decreases as the TX-distance increases. Furthermore, when the second person touches the subject a leakage path is created and, as a consequence, part of the signal is de-phased and attenuated. Without taking into account the propagative nature of the body channel, i.e., using simple RC models as found often in the literature [31], the explanation of these cases would be non-trivial.

Given the advantages of BCC, since the practical use of any CC device, such as the case-use *Live Wire*, is the final application, a series of critical cases were investigated. In particular, the characterization of BCC devices operating in presence of other subjects is an aspect poorly analyzed in the literature [3]–[6]. Therefore, in this work, we investigated the case of No Touch Propagation, i.e., when a subject touches the TX, but another person at a given distance wears the RX, without being in contact, as shown in Fig. 7(h). The SNR values measured moving the subject with the RX in the four directions around the TX, for distances from 5 cm to 120 cm, are presented in Fig. 12. In all the four direction the signal strength reduces while the TX-RX distance increases. The SNR values are not defined for d > 90 cm, and hence no communication occurs. From Fig. 12 it can be noticed that the SNR varies of $\sim \pm 12$ dB in the four directions, which implies that the environment and the return path through the parasitic capacitance may have a strong influence on the body channel propagation.

The results for the chain from one to six people are shown in Fig. 13. The contact between different people does not significantly degrade the signal. In fact, it retains an SNR between 30 dB and 40 dB, which is sufficient to discriminate the signal from the noise at the RX site. As a matter of
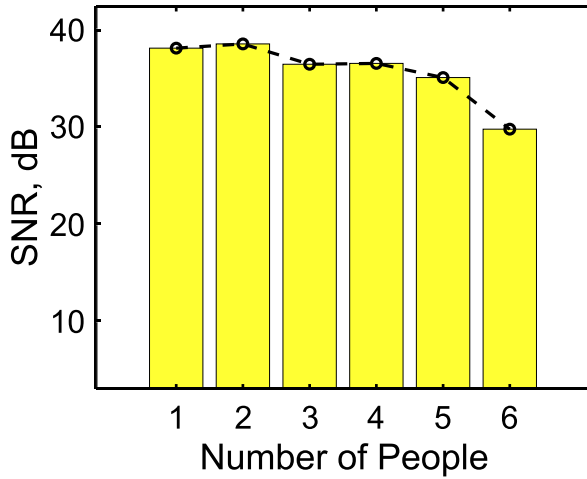
FIGURE 13. SNR levels measured for a chain of one to six people, in contact, interposed between the TX and RX.

FIGURE 14. a) Comparison of the PER for the air and BCC transmission mechanisms vs. the TX-RX distance. b) Comparison of the TER for the air and BCC transmission mechanisms vs. the TX-RX distance.

fact, the contact between different people degrades the signal. Considering our periodic transmission line model (see Fig. 3), in the case of the people chain, the resulting propagation channel is composed by unit cells having a slightly variable skin properties, which determine this reduction in the signal strength.

C. COMMUNICATION PERFORMANCES

The experimental assessment of the SNR allows to measure the signal levels, given a constant noise level. The results in Fig.s 10-13 provided a useful feedback about the capability of the proposed mathematical framework for describing the physical mechanism of BCC. However, the SNR does not provide information about the communication performances. Therefore, in order to assess the actual communication between TX and RX, the PER and TER are evaluated in the same experimental configurations (see Fig. 7).

The quantification of PER and TER for the case of air vs. body transmission (i.e., cases of Fig. 7(a)-(c)) confirms the necessity of the body presence to ensure the communication, coherently with the proposed model, as can be inferred from Fig. 14. Indeed, in a way similar to the SNR findings from Fig. 10, when the transmitter and the receiver are in contact to each other (e.g. less than 1 cm of distance) the signal can couples by the electrostatic near-field in air and through human tissues. However, when the distance slightly increases and overcome 5 cm, the communication is guaranteed by the guided-transmission in the body. Therefore, the PER in the air channel can be only evaluated when TX and RX are in contact as shown in Fig. 14(a). When the signal is confined in the skin layer, due to the relatively constant SNR levels, for distances up to 15 cm, the PER reaches a maximum of 0.2. As regards the TER values, shown in Fig. 14(b), it can be noticed that in air the error are higher than those achieved for on-body propagation, except when the TX and RX are in close contact.
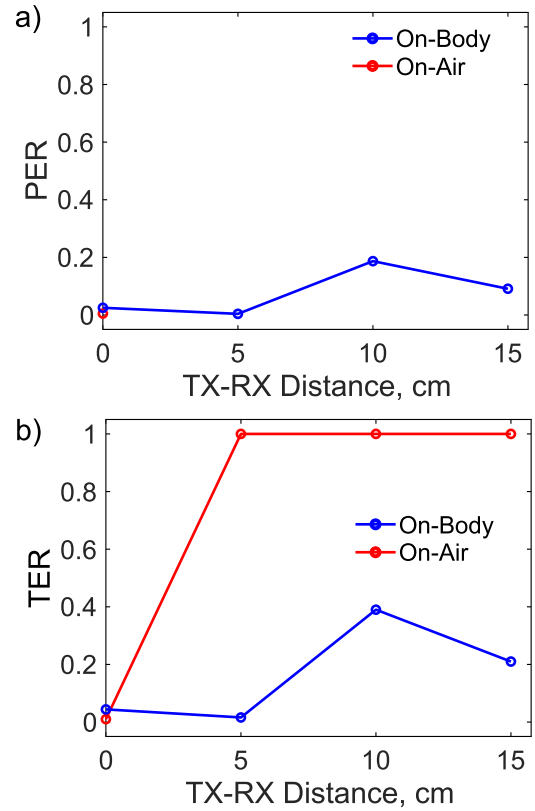
In the most critical cases of No Touch Propagation tests, i.e., the cases Fig. 7(e)-(g), interesting differences across the configurations arises. In particular, the PER values are comprised between 0 and 0.2, as shown in Fig. 15(a). The highest value of 0.6 is reached when the shielding is due to the self hand of the subject at a distance of 2 cm from the TX. Despite this outlier, the PER attenuates with the TX-hand distance (about a 50% reduction in 3 cm). As regards the TER values, shown in Fig. 15(b), it can be noticed that the TER is maximum for TX-hand distance up to 2 cm, and then reduces of more than 60%. This implies that the number of correct packets, with respect to the total number of packet sent, is lower than that achieved in the No Self Hand cases, i.e. Fig. 7(h) and 7(i). For the cases of body shielding, the TER values (Fig. 15(b)) show an overall downward trend with increasing distance. It emerges that the hand positioning on the receiver has an effect in all the configurations analyzed, but when the hand-RX distance is zero, or very small, such effect still enables communication only if the hand touching RX is of a second person and no touch occurs. When the hand is distanced more than 5 cm TER values are in the expected range below 40%.

Finally, the evaluation of PER and TER was performed for the case of people chain. From the findings of Fig. 16, it can be underlined that the PER oscillates around 0 and 0.1 for an increasing number of people and hence, the number
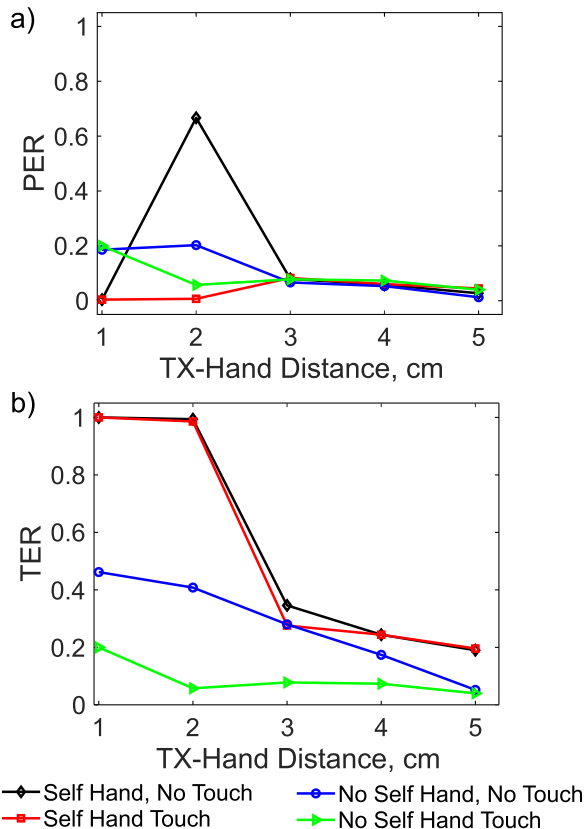
FIGURE 15. a) PER measurements in the case of body shielding evaluation. b) TER measurements in the case of body shielding evaluation. (Self Hand, No Touch - Fig. 7(d); Self Hand, Touch - Fig. 7(e); No Self Hand, No Touch - Fig. 7(h); No Self Hand, Touch - Fig. 7(i).
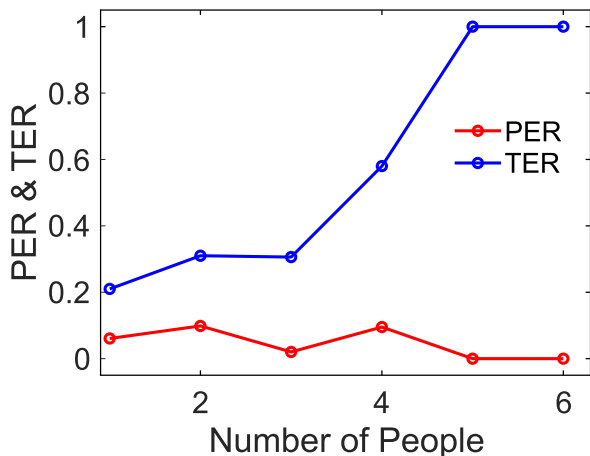

FIGURE 16. Packet and Total Error Rates (PER, TER respectively) values assessed for a chain of one to six people, in contact, interposed between the TX and RX.

of uncorrect packets about a tenth of the number of correct ones. However, as result from the TER values, the number of correct packets over the total number of packet sent, decreases as the number of people increases. All these findings underline that it is possible to establish the communication using the body as transmission medium, and the case-use

device *Live Wire* is capable of that, but still exist some critical cases which may hamper the use of BCC in practice. These limitations can be understood and studied using the proposed mathematical framework to design or enhance the performances of a given CC device for BCC.

VI. CONCLUSION

This work dealt with the problem of the development and validation of a transmission line model for BCC. A novel periodic transmission line model was developed in order to describe the signal propagation and to establish a quantitative and general basis for BCC. The unknown model parameters were estimated by fitting the experimental data of bio-impedances measurements performed on ten subjects. The novel finite periodic TLM allowed to describe, from 50 kHz to 1 MHz, the frequency response of the body impedances with average errors of 4° and 30 Ω for the phase angle and impedance modulus, respectively. The model was successfully evaluated by testing the case-use capacitive ground-referred device called *Live Wire* finding good correlation between experimental and calculated data. The agreement is within ±3%, which is remarkable, given the intrinsic variability and the 30% uncertainty associated to the parameters related to signal transmission. The proposed model could be used to enhance the performances of capacitive BCC devices. The signal propagation through the human body channel was characterized using the *Live Wire* device in several scenarios. The communication performances were quantified in terms of SNR. The differences between the over-the-air channel transmission and the on-body propagation were analyzed. The BCC mechanism ensure a 40 dB SNR level when the body channel acts as a wire conveying the information from the TX to the RX. Furthermore, the signal decay was tested when a chain of people constitutes the channel, finding a 12.5% reduction per three people. Some critical case are considered. In particular, the body shielding (or shunt) effects and the No Touch Propagation are commented and discussed relying on the proposed model.

The proposed TLM model is a novel distributed model which account for the finite size of the body channel while including the hardware features of TX and RX. Several key points of this paper need to be further addressed in future works. The periodic transmission line model of the skin and the related circuital representation could be used to design impedance-matching networks at both the TX output and the RX input [3], to enhance the overall performance of a BCC system. As underlined by both the model and the experimental analysis, the proposed mathematical framework can be used to investigate the critical cases of communication between TX and RX in CC systems. As an example, the proposed model can be used to investigate frequency hopping techniques for the performance enhancement [6], [33], [60]. Moreover, since BCC is intended for wearable biomedical applications the type electrodes could be modified to turn the device to a truly wearable piece of electronics. An interesting and

appealing opportunity is represented by the investigation of textile electrodes, either metallic or polymer based [61], [62], already used for biopotentials acquisition [55], [63], [64]. In particular, the polymer-based electrodes are interesting because of their non-metallic nature which could hamper the signal transmission at the selected working frequencies. Finally, the proposed circuital scheme and the TLM model can be used to investigate this scenario.

ACKNOWLEDGMENT

REFERENCES

[1] T. G. Zimmerman, "Personal area networks (PAN): Near-eld intra-body communication," M.S. thesis, Massachusetts Inst. Technol., Cambridge, MA, USA, 1995.

[2] T. G. Zimmerman, "Personal area networks: Near-field intrabody communication," *IBM Syst. J.*, vol. 35, no. 3.4, pp. 609–617, 1996.

[3] D. Naranjo-Hernández, A. Callejón-Leblic, V. Z. L. Vasić, M. Seyedi, and Y.-M. Gao, "Past results, present trends, and future challenges in intrabody communication," *Wireless Commun. Mobile Comput.*, vol. 2018, pp. 1–39, Mar. 2018.

[4] M. Seyedi, B. Kibret, D. T. H. Lai, and M. Faulkner, "A survey on intrabody communications for body area network applications," *IEEE Trans. Biomed. Eng.*, vol. 60, no. 8, pp. 2067–2079, Aug. 2013.

[5] J. F. Zhao, X. M. Chen, B. D. Liang, and Q. X. Chen, "A review on human body communication: Signal propagation model, communication performance, and experimental issues," *Wireless Commun. Mobile Comput.*, vol. 2017, pp. 1–15, Oct. 2017.

[6] W. J. Tomlinson, S. Banou, C. Yu, M. Stojanovic, and K. R. Chowdhury, "Comprehensive survey of galvanic coupling and alternative intra-body communication technologies," *IEEE Commun. Surveys Tuts.*, vol. 21, no. 2, pp. 1145–1164, 2nd Quart., 2019.

[7] K. Fujii, M. Takahashi, and K. Ito, "Electric field distributions of wearable devices using the human body as a transmission channel," *IEEE Trans. Antennas Propag.*, vol. 55, no. 7, pp. 2080–2087, Jul. 2007.

[8] J. Bae, H. Cho, K. Song, H. Lee, and H.-J. Yoo, "The signal transmission mechanism on the surface of human body for body channel communication," *IEEE Trans. Microw. Theory Techn.*, vol. 60, no. 3, pp. 582–593, Mar. 2012.

[9] J. Bae and H.-J. Yoo, "The effects of electrode configuration on body channel communication based on analysis of vertical and horizontal electric dipoles," *IEEE Trans. Microw. Theory Techn.*, vol. 63, no. 4, pp. 1409–1420, Apr. 2015.

[10] N. B. Asan, C. P. Penichet, S. Redzwan Mohd Shah, D. Noreland, E. Hassan, A. Rydberg, T. J. Blokhuis, T. Voigt, and R. Augustine, "Data packet transmission through fat tissue for wireless IntraBody networks," *IEEE J. Electromagn., RF Microw. Med. Biol.*, vol. 1, no. 2, pp. 43–51, Dec. 2017.

[11] N. Asan, E. Hassan, J. Shah, D. Noreland, T. Blokhuis, E. Wadbro, M. Berggren, T. Voigt, and R. Augustine, "Characterization of the fat channel for intra-body communication at R-band frequencies," *Sensors*, vol. 18, no. 9, p. 2752, Aug. 2018.

[12] N. B. Asan, E. Hassan, M. D. Perez, S. R. Mohd Shah, J. Velander, T. J. Blokhuis, T. Voigt, and R. Augustine, "Assessment of blood vessel effect on fat-intrabody communication using numerical and *ex-vivo* models at 2.45 GHz," *IEEE Access*, vol. 7, pp. 89886–89900, 2019.

[13] J.-H. Hwang, T.-W. Kang, J.-H. Kwon, and S.-O. Park, "Effect of electromagnetic interference on human body communication," *IEEE Trans. Electromagn. Compat.*, vol. 59, no. 1, pp. 48–57, Feb. 2017.

[14] R. Cavallari, F. Martelli, R. Rosini, C. Buratti, and R. Verdone, "A survey on wireless body area networks: Technologies and design challenges," *IEEE Commun. Surveys Tuts.*, vol. 16, no. 3, pp. 1635–1657, 3rd Quart., 2014.

[15] *IEEE Standard for Local and Metropolitan Area Networks—Part 15.6: Wireless Body Area Networks*, IEEE Standard 802.15.6-2012, Feb. 2012.

[16] T. Handa, S. Shoji, S. Ike, S. Takeda, and T. Sekiguchi, "A very low-power consumption wireless ECG monitoring system using body as a signal transmission medium," in *Proc. Int. Solid State Sens. Actuators Conf. (Transducers)*, vol. 2, Jun. 1997, pp. 1003–1006.

[17] Z. Lucev, I. Krois, and M. Cifrek, "Application of wireless intrabody communication system to muscle fatigue monitoring," in *Proc. IEEE Instrum. Meas. Technol. Conf.*, May 2010, pp. 1624–1627.

[18] K. Hachisuka, A. Nakata, T. Takeda, Y. Terauchi, K. Shiba, K. Sasaki, H. Hosaka, and K. Itao, "Development and performance analysis of an intra-body communication device," in *12th Int. Conf. Solid-State Sens., Actuators Microsyst. Dig. Tech. Papers (TRANSDUCERS)*, vol. 2, Jun. 2003, pp. 1722–1725.

[19] L. Bereuter, M. Gysin, T. Kueffer, M. Kucera, T. Niederhauser, J. Fuhrer, P. Heinisch, A. Zurbuchen, D. Obrist, H. Tanner, and A. Haeberlin, "Leadless dual-chamber pacing: A novel communication method for wireless pacemaker synchronization," *JACC, Basic Transl. Sci.*, vol. 3, no. 6, pp. 813–823, 2018.

[20] Y. Tseng, C. Su, and Y. Ho, "Evaluation and verification of channel transmission characteristics of human body for optimizing data transmission rate in electrostatic-coupling intra body communication system: A comparative analysis," *PLoS ONE*, vol. 11, no. 2, Feb. 2016, Art. no. e0148964.

[21] V. Varga, G. Vakulya, A. Sample, and T. R. Gross, "Enabling interactive infrastructure with body channel communication," in *Proc. ACM Interact., Mobile, Wearable Ubiquitous Technol.*, vol. 1, no. 4, p. 169, 2018.

[22] V. Varga, M. Wyss, G. Vakulya, A. Sample, and T. R. Gross, "Designing groundless body channel communication systems: Performance and implications," in *Proc. 31st Annu. ACM Symp. Interface Softw. Technol. (UIST)*, 2018, pp. 683–695.

[23] M. Fukumoto and M. Shinagawa, "Carpetlan: A novel indoor wireless (-like) networking and positioning system," in *Proc. Int. Conf. Ubiquitous Comput.* Berlin, Germany: Springer, 2005, pp. 1–18.

[24] Y. Kado, T. Kobase, T. Yanagawa, T. Kusunoki, M. Takahashi, R. Nagai, O. Hiromitsu, A. Hataya, H. Simasaki, and M. Shinagawa, "Human-area networking technology based on near-field coupling transceiver," in *Proc. IEEE Radio Wireless Symp.*, Jan. 2012, pp. 119–122.

[25] H. Wang, X. Tang, C. S. Choy, and G. E. Sobelman, "Cascaded network body channel model for intrabody communication," *IEEE J. Biomed. Health Informat.*, vol. 20, no. 4, pp. 1044–1052, Jul. 2016.

[26] W. J. Tomlinson, S. Banou, S. Blechinger-Slocum, C. Yu, and K. R. Chowdhury, "Body-guided galvanic coupling communication for secure biometric data," *IEEE Trans. Wireless Commun.*, vol. 18, no. 8, pp. 4143–4156, Aug. 2019.

[27] M. Särestöniemi, M. Hämäläinen, and J. Iinatti, "An overview of the electromagnetic simulation-based channel modeling techniques for wireless body area network applications," *IEEE Access*, vol. 5, pp. 10622–10632, 2017.

[28] A. K. Teshome, B. Kibret, and D. T. H. Lai, "Galvanically coupled intrabody communications for medical implants: A unified analytic model," *IEEE Trans. Antennas Propag.*, vol. 64, no. 7, pp. 2989–3002, Jul. 2016.

[29] K. Doi, K. Koyama, Y. Suzuki, and T. Nishimura, "Development of the communication module used human body as the transmission line," in *Proc. Hum. Interface Symp.*, 2001, pp. 389–392.

[30] M. S. Wegmueller, A. Kuhn, J. Froehlich, M. Oberle, N. Felber, N. Kuster, and W. Fichtner, "An attempt to model the human body as a communication channel," *IEEE Trans. Biomed. Eng.*, vol. 54, no. 10, pp. 1851–1857, Oct. 2007.

[31] R. Xu, H. Zhu, and J. Yuan, "Electric-field intrabody communication channel modeling with finite-element method," *IEEE Trans. Biomed. Eng.*, vol. 58, no. 3, pp. 705–712, Mar. 2011.

[32] M. A. Callejon, L. M. Roa, J. Reina-Tosina, and D. Naranjo-Hernandez, "Study of attenuation and dispersion through the skin in intrabody communications systems," *IEEE Trans. Inf. Technol. Biomed.*, vol. 16, no. 1, pp. 159–165, Jan. 2012.

[33] N. Cho, L. Yan, J. Bae, and H.-J. Yoo, "A 60 kb/s–10 Mb/s adaptive frequency hopping transceiver for interference-resilient body channel communication," *IEEE J. Solid-State Circuits*, vol. 44, no. 3, pp. 708–717, Mar. 2009.

[34] K. F. K. Ito and M. Takahashi, "Transmission mechanism of wearable devices using the human body as a transmission channel," in *Antennas and Propagation for Body-Centric Wireless Communications*, Y. H. S Hall, Ed. London, U.K.: Artech House, 2012, ch. 4, pp. 65–92.

[35] M. Crepaldi, G. Zini, A. Maviglia, A. Barcellona, A. Merello, and L. Brayda, "Live wire: Body channel communication as a high impedance and frequency-scaled impulse radio," in *Proc. IEEE Biomed. Circuits Syst. Conf. (BioCAS)*, Oct. 2017, pp. 1–4.

[36] G. Franceschetti, *Electromagnetics: Theory, Techniques, and Engineering Paradigms*. New York, NY, USA: Springer, 2013.

[37] C. Christopoulos, *The Transmission-Line Modeling Method: TLM*. London, U.K.: Oxford Univ. Press, 1995.

[38] M. N. Sadiku and C. K. Alexander, *Fundamentals of Electric Circuits*. New York, NY, USA: McGraw-Hill, 2007.

[39] S. Gabriel, R. W. Lau, and C. Gabriel, "The dielectric properties of biological tissues: III. Parametric models for the dielectric spectrum of tissues," *Phys. Med. Biol.*, vol. 41, no. 11, p. 2271, 1996.

[40] J. Clegg and M. Robinson, "A genetic algorithm for optimizing multi-pole debye models of tissue dielectric properties," *Phys. Med. Biol.*, vol. 57, no. 19, p. 6227, 2012.

[41] S. Salahuddin, E. Porter, F. Krewer, and M. O' Halloran, "Optimised analytical models of the dielectric properties of biological tissue," *Med. Eng. Phys.*, vol. 43, pp. 103–111, May 2017.

[42] D. M. Pozar, *Microwave Engineering*. Hoboken, NJ, USA: Wiley, 2009.

[43] R. Plonsey and R. E. Collin, *Principles and Applications of Electromagnetic Fields*. New York, NY, USA: McGraw-Hill, 1961.

[44] M. Crepaldi, A. Barcellona, G. Zini, A. Ansaldo, P. M. Ros, A. Sanginario, C. Cuccu, D. De Marchi, and L. Brayda, "Live wire—A low-complexity body channel communication system for landmark identification," *IEEE Trans. Emerg. Topics Comput.*, early access, May 28, 2020, doi: 10.1109/TETC.2020.2996280.

[45] D. P. Lindsey, E. L. McKee, M. L. Hull, and S. M. Howell, "A new technique for transmission of signals from implantable transducers," *IEEE Trans. Biomed. Eng.*, vol. 45, no. 5, pp. 614–619, May 1998.

[46] J. Mao, H. Yang, Y. Lian, and B. Zhao, "A self-adaptive capacitive compensation technique for body channel communication," *IEEE Trans. Biomed. Circuits Syst.*, vol. 11, no. 5, pp. 1001–1012, Oct. 2017.

[47] S.-J. Song, N. Cho, and H.-J. Yoo, "A 0.2-mW 2-Mb/s digital transceiver based on wideband signaling for human body communications," *IEEE J. Solid-State Circuits*, vol. 42, no. 9, pp. 2021–2033, Sep. 2007.

[48] H. Lee, K. Lee, S. Hong, K. Song, T. Roh, J. Bae, and H.-J. Yoo, "A 5.5 mW IEEE-802.15.6 wireless body-area-network standard transceiver for multichannel electro-acupuncture application," in *IEEE Int. Solid-State Circuits Conf. (ISSCC) Dig. Tech. Papers*, Feb. 2013, pp. 452–453.

[49] H.-Y. Shih, Y.-C. Chang, C.-W. Yang, and C.-C. Chen, "A low-power and small chip-area multi-rate human body communication DPFSK transceiver for wearable devices," *IEEE Trans. Circuits Syst. II, Exp. Briefs*, vol. 67, no. 7, pp. 1234–1238, Jul. 2020.

[50] S. Maity, B. Chatterjee, G. Chang, and S. Sen, "BodyWire: A 6.3-pJ/b 30-Mb/s −30-dB SIR-tolerant broadband interference-robust human body communication transceiver using time domain interference rejection," *IEEE J. Solid-State Circuits*, vol. 54, no. 10, pp. 2892–2906, Oct. 2019.

[51] K. Lin, B. Wang, X. Zhang, X. Wang, T. Ouyang, and H. Chen, "A novel low-power compact WBS human body channel receiver for wearable vital signal sensing application in wireless body-area network," *Microsyst. Technol.*, vol. 23, no. 10, pp. 4459–4473, Oct. 2017.

[52] L. Beckman, C. Neuhaus, G. Medrano, N. Jungbecker, M. Walter, T. Gries, and S. Leonhardt, "Characterization of textile electrodes and conductors using standardized measurement setups," *Physiol. Meas.*, vol. 31, no. 2, pp. 233–247, 2010.

[53] M. Di Rienzo, V. Racca, F. Rizzo, B. Bordoni, G. Parati, P. Castiglioni, P. Meriggi, and M. Ferratini, "Evaluation of a textile-based wearable system for the electrocardiogram monitoring in cardiac patients," *EP Europace*, vol. 15, no. 4, pp. 607–612, Apr. 2013.

[54] G. A. Álvarez-Botero, Y. K. Hernández-Gómez, C. E. Telléz, and J. F. Coronel, "Human body communication: Channel characterization issues," *IEEE Instrum. Meas. Mag.*, vol. 22, no. 5, pp. 48–53, Oct. 2019.

[55] D. Pani, A. Dessì, J. F. Saenz-Cogollo, G. Barabino, B. Fraboni, and A. Bonfiglio, "Fully textile, PEDOT: PSS based electrodes for wearable ECG monitoring systems," *IEEE Trans. Biomed. Eng.*, vol. 63, no. 3, pp. 540–549, Mar. 2016.

[56] Ø. G. Martinsen, S. Grimnes, and E. Haug, "Measuring depth depends on frequency in electrical skin impedance measurements," *Skin Res. Technol.*, vol. 5, no. 3, pp. 179–181, Aug. 1999.

[57] T. Yamamoto and Y. Yamamoto, "Electrical properties of the epidermal stratum corneum," *Med. Biol. Eng.*, vol. 14, no. 2, pp. 151–158, Mar. 1976.

[58] B. Ivšić, G. Golemac, and D. Bonefačić, "Performance of wearable antenna exposed to adverse environmental conditions," in *Proc. ICECom*, Oct. 2013, pp. 1–4.

[59] C. Hertleer, A. Van Laere, H. Rogier, and L. Van Langenhove, "Influence of relative humidity on textile antenna performance," *Textile Res. J.*, vol. 80, no. 2, pp. 177–183, Jan. 2010.

[60] M. Li, Y. Song, Y. Hou, N. Li, Y. Jiang, M. Sulaman, and Q. Hao, "Comparable investigation of characteristics for implant intra-body communication based on galvanic and capacitive coupling," *IEEE Trans. Biomed. Circuits Syst.*, vol. 13, no. 6, pp. 1747–1758, Dec. 2019.

[61] J.-H. Moon, D. H. Baek, Y. Y. Choi, K. H. Lee, H. C. Kim, and S.-H. Lee, "Wearable polyimide–PDMS electrodes for intrabody communication," *J. Micromech. Microeng.*, vol. 20, no. 2, Feb. 2010, Art. no. 025032.

[62] A. Achilli, D. Pani, and A. Bonfiglio, "Characterization of screen-printed textile electrodes based on conductive polymer for ECG acquisition," in *Proc. Comput. Cardiol. Conf. (CinC)*, Sep. 2017, pp. 1–4.

[63] D. Pani, A. Achilli, and A. Bonfiglio, "Survey on textile electrode technologies for electrocardiographic (ECG) monitoring, from metal wires to polymers," *Adv. Mater. Technol.*, vol. 3, no. 10, Oct. 2018, Art. no. 1800008.

[64] D. Pani, A. Achilli, A. Spanu, A. Bonfiglio, M. Gazzoni, and A. Botter, "Validation of polymer-based screen-printed textile electrodes for surface EMG detection," *IEEE Trans. Neural Syst. Rehabil. Eng.*, vol. 27, no. 7, pp. 1370–1377, Jul. 2019.
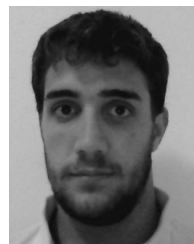
MATTEO BRUNO LODI (Graduate Student Member, IEEE) was born in Cagliari, in January 1994. He received the bachelor's degree in biomedical engineering from the University of Cagliari, in 2016, and the master's degree in biomedical engineering from Politecnico di Torino, in 2018. He is currently pursuing the Ph.D. degree in electronic engineering and computer science with the University of Cagliari. His research activity deals with the modeling of bio-electromagnetic phenomena, the study, manufacturing and synthesis of magnetic biomaterials for tissue engineering applications, and the use of microwave for biotechnology and environmental applications.

NICOLA CURRELI received the M.Sc. degree in bioengineering from the University of Genoa, Genoa, Italy, in 2016, and the Ph.D. degree in electronic engineering from the University of Cagliari, Cagliari, Italy, and the Italian Institute of Technology, Genoa, in 2020. In 2019, he was a Visiting Researcher with the Physics and Mechanical Engineering Department, Columbia University, New York City, New York, USA. He is currently a post-doc with the Italian Institute of Technology in the WP12 (Energy storage) of the Graphene Core 2 project - Graphene flagship. His research activity is focused on the study of 2D materials and their application in the fields of electronics and optics.

ALESSANDRO FANTI (Member, IEEE) received the Laurea degree in electronic engineering and the Ph.D. degree in electronic engineering and computer science from the University of Cagliari, Cagliari, Italy, in 2006 and 2012, respectively. He worked as Postdoctoral Fellow in the Electromagnetic Group, University of Cagliari, from 2013 to 2016, where he is currently an Assistant Professor. His research activity involves the use of numerical techniques for modes computation of guiding structures, optimization techniques, analysis and design of waveguide slot arrays, analysis and design of patch antennas, radio propagation in urban environment, modeling of bio-electromagnetic phenomena, microwave exposure systems for biotechnology and bio-agriculture. He is an Associate Editor of the IEEE JOURNAL OF ELECTROMAGNETICS, RF AND MICROWAVES IN MEDICINE AND BIOLOGY (J-ERM).

CLAUDIA CUCCU received the bachelor's degree in biomedical engineering from the University of Cagliari, in 2016, and the master's degree in biomedical engineering with major in biomedical instrumentation from Politecnico di Torino, in October 2019, discussing a thesis entitled: "Modeling and characterization of a body channel communication system". Her main research interests are the study of biomedical signal processing, the modeling and investigation body channel communication, and bionanotechnologies.

DANILO PANI (Senior Member, IEEE) graduated in electronic engineering *(magna cum laude)* and the Ph.D. degree in electronic and computer engineering from the University of Cagliari, Italy, in 2002 and 2006, respectively. He is currently an Associate Professor of biomedical engineering with the University of Cagliari, Italy. His research interests are in the field of biomedical signal analysis and processing and medical devices. His main achievements regard non-invasive fetal ECG, textile electrodes, real-time neural signal processing, and telehealth systems. He is author of more than 90 scientific publications and five patents.

ALESSANDRO SANGINARIO (Member, IEEE) received the master's degree in biomedical engineering and the Ph.D. degree in physics from the Politecnico di Torino, in 2006 and 2011, respectively. From 2006 to 2007, he was with LATEMAR Project. He is with the Chilab Material and Microsystems Laboratory, Politecnico di Torino, working on the LATEMAR Project. He was a Visiting Ph.D. Student with the Vestfold University College, Norway, during his Ph.D. period. Since 2012, he has held a junior postdoctoral position at the Center for Space Human Robotics, Istituto Italiano di Tecnologia. His research interests concern microelectromechanical systems and advanced sensors, in particular, for biomedical applications.

ANDREA SPANU (Member, IEEE) received the master's and Ph.D. degrees in bioengineering from the University of Genova, in 2011 and 2015, respectively. He spent his postdoc career between University of Cagliari (Department of Electrical and Electronic Engineering), the Nanoscale fabrication group at the IBM Almaden Research Center, San Jose, California, and Bruno Kessler Foundation, Trento, Italy, from January 2018 to January 2019, where he held a CARITRO grant for young researchers with a project titled Innovative organic electronic devices and 3D microelectrodes for brain-in-a-dish applications. In February 2019, he joined the Department of Electrical and Electronic Engineering, University of Cagliari, as an Assistant Professor. His research interests range from the integration of organic electronics and (in vitro and in vivo) electrophysiology, innovative devices for Brain on a Dish applications, smart textiles and tattoo electronics for tactile applications, and bio-signals acquisition.

PAOLO MOTTO ROS (Member, IEEE) is currently a Senior Postdoc Researcher with Dipartimento di Elettronica e Telecomunicazioni, Politecnico di Torino, Torino, Italy, with the MiNES (Microand Nano Electronic Systems) group. He received the degree in electronic engineering and the Ph.D. degree in electronic engineering from the Politecnico di Torino, Torino, Italy, in 2005 and 2009, respectively. From 2009 to 2012, he was with the Neuronica Laboratory (Dipartimento di Elettronica, Politecnico di Torino) as a postdoctoral researcher, working on assistive technologies, computer vision and learning machines projects (jointly with, 2006–2011, Istituto Nazionale Fisica Nucleare, INFN, Italy). From 2012 to 2019, he was with Istituto Italiano di Tecnologia (Center for Space Human Robotics, CSHR, Torino, Italy, and, since 2016, Electronic Design Laboratory, EDL, Genova, Italy) as senior (since 2014) Postdoctoral Researcher, working on bio-inspired electronics for biomedical and humanoid robotic applications. He joined the Politecnico di Torino, Dipartimento di Elettronica e Telecomunicazioni, in 2019. He is a member of the Circuits and Systems (CAS) society; he was a member of the organizing staff of the IEEE BioCAS 2017 conference, and a member of the organizing committee of the IEEE ICECS 2019 conference. He counts >40 publications. His current research interests include: event-driven digital integrated circuits, architectures, and systems; low-power smart sensor networks; bio-inspired electronics; biomedical and humanoid robotic applications.

MARCO CREPALDI (Member, IEEE) received the degree *(summa cum laude)* in engineering and the Ph.D. degree in electronic engineering from the Politecnico di Torino (Polito), Turin, Italy, in 2005 and 2009, respectively. In 2008, he was a Visiting Scholar with the Electrical Engineering Department, Columbia University, New York City. After the Ph.D., he held a postdoctoral position at the VLSI Lab, Electrical Engineering Department, PoliTo and, then, at the Istituto Italiano di Tecnologia (IIT)@PoliTo Center for Space Human Robotics. From 2013 to 2015, he was scientific responsible for the Istituto Italiano di Tecnologia of the FP7 Project SMArt system Co-design. He is currently a Coordinator with the Electronics Design Lab, IIT Center for Human Technology, Genoa. His scientific activity is related to the analysis, simulation, and development of the integrated event-driven and all-digital impulse-radio ultra-wide band systems. He is a member of the Circuits and Systems Society.

DANILO DEMARCHI (Senior Member, IEEE) received the degree in engineering and the Ph.D. degree in electronics engineering from the Politecnico di Torino, Italy, in 1991 and 1995, respectively. His full position as an Associate Professor at Politecnico di Torino, Department of Electronics and Telecommunications and a Visiting Professor at EPFL Lausanne and at Tel Aviv University. He was a Visiting Scientist, MIT, in August 2018, and the Harvard Medical School. He is also leading the MiNES (Microand Nano Electronic Systems) Laboratory, Politecnico di Torino. He is the author and coauthor of three patents and more than 200 scientific publications in international journals and peer-reviewed conference proceedings. He is also a member of the BioCAS Technical Committee and an Associate Editor of the IEEE Transactions on Biomedical Circuits and Systems (TBioCAS), the IEEE Sensors Journal, and *Bio Nano Science* journal (Springer). He was a General Chair of the Biomedical Circuits and Systems (BioCAS) Conference, Torino, in 2017, and the Founder of the IEEE Circuits and Systems for the Food Chain (FoodCAS) Workshop.

GIUSEPPE MAZZARELLA (Senior Member, IEEE) graduated with *(summa with laude)* in electronic engineering from the Universit Federico II of Naples, in 1984, and the Ph.D. degree in electronic engineering and computer science, in 1989. In 1990, he became an Assistant Professor at the Dipartimentodi Ingegneria Elettronica, Università Federico II of Naples. Since 1992, he has been with the Dipartimento diIngegneria Elettrica ed Elettronica of the Università di Cagliari, first as an Associate Professor and then, since 2000, as a Full Professor, teaching courses in electromagnetics, microwave, antennas and remote sensing. His research activity has focused mainly on: efficient design of large arrays of slots, power synthesis of array factor, with emphasis on inclusion of constraints, microwave holography techniques for the diagnosis of large reflector antennas, use of evolutionary programming for the solution of inverse problems, in particular problems of synthesis of antennas and periodic structures. He is author (or coauthor) of over 70 papers in international journals, and is a reviewer for many EM journals.

● ● ●